

Article

Development and Validation of an Electromagnetic Induction-Based Thermal Propagation Test Method for Large-Format Lithium-Ion Battery Systems

Changyong Jin ¹, Jiangna Gu ², Chengshan Xu ¹, Wanlin Wang ², Lirong Liu ^{2,*} and Xuning Feng ^{1,*}

¹ State Key Laboratory of Intelligent Green Vehicle and Mobility (SKLIGVM), School of Vehicle and Mobility, Tsinghua University, Beijing 100084, China; jinchangyong1@mail.tsinghua.edu.com (C.J.)

² Farasis Energy (GanZhou) Co., Ltd., Ganzhou 341000, China

* Correspondence: lrliu@farasisenergy.com (L.L.); fxn17@mail.tsinghua.edu.cn (X.F.)

Abstract: This study establishes a standardized framework for thermal propagation test in nickel-7 lithium-ion battery systems through a high-frequency electromagnetic induction heating method. The non-intrusive triggering mechanism enables precise thermal runaway initiation within two seconds through localized eddy current heating ($>1200\text{ }^{\circ}\text{C}$), validated through cell-level tests with 100% success rate across diverse trigger positions. System-level thermal propagation tests were conducted on two identical battery boxes. The parallel experiments revealed distinct propagation patterns influenced by system sealing quality. In the inadequately sealed system (Box 01), flame formation led to accelerated thermal propagation through enhanced convective and radiative heat transfer. In contrast, the well-sealed system (Box 02) maintained an oxygen-deficient environment, resulting in a controlled sequential propagation pattern. The testing methodology incorporating dummy modules proved efficient for validating thermal protection strategies while optimizing costs. This study contributes to a deeper understanding of thermal runaway propagation mechanisms and the development of standardized testing protocols for large-format battery systems.



Academic Editor: Prodip K. Das

Received: 21 February 2025

Revised: 23 March 2025

Accepted: 4 April 2025

Published: 9 April 2025

Citation: Jin, C.; Gu, J.; Xu, C.; Wang, W.; Liu, L.; Feng, X. Development and Validation of an Electromagnetic Induction-Based Thermal Propagation Test Method for Large-Format Lithium-Ion Battery Systems. *Batteries* **2025**, *11*, 148. <https://doi.org/10.3390/batteries11040148>

Copyright: © 2025 by the authors. Licensee MDPI, Basel, Switzerland. This article is an open access article distributed under the terms and conditions of the Creative Commons Attribution (CC BY) license (<https://creativecommons.org/licenses/by/4.0/>).

1. Introduction

With the acceleration of global transportation electrification and the decarbonization of energy, lithium-ion batteries (LIBs), due to their superior performance and potential, have become a core technology driving these changes. LIBs offer high energy density, long cycle life, low self-discharge rates, and relatively low maintenance requirements, which make them widely used in electric vehicles, portable electronic devices, and renewable energy storage systems [1]. In the context of transportation electrification, LIBs offer an effective solution to reduce dependency on fossil fuels and lower emissions. However, the pursuit of higher specific energy (i.e., higher energy storage capacity) often comes at the expense of battery system safety. Increasing energy density may require trade-offs in design and material selection, which can elevate the risk of thermal runaway (TR), a critical challenge in battery development [2,3].

While high-specific-energy LIBs meet the growing demand for enhanced energy density, they also pose significant safety concerns. These batteries often employ cathode materials with higher nickel content, such as nickel manganese cobalt (NMC) or nickel

cobalt aluminum (NCA), to enhance capacity and energy density. However, high-nickel cathode materials have inherently lower thermal stability, making them prone to TR [4,5]. Studies have indicated that at high temperatures, high-nickel cathode materials undergo oxygen release and structural changes, resulting in lower TR temperatures and faster thermal propagation (TP) [6,7]. Compared to lithium iron phosphate (LFP) batteries, high-specific-energy batteries show significantly reduced thermal stability and lower resistance to thermal abuse [8–10]. When TR occurs, the associated heat generation, gas release, and venting are more intense, increasing the risk of fire and, in severe cases, explosion within the battery module or pack.

Ensuring the safety of high-specific-energy LIBs requires efforts at both the manufacturing and system levels [11]. From a manufacturing perspective, improving process quality (e.g., reducing impurities, optimizing material synthesis processes, etc.), and enhancing electrolytes and current collectors can decrease the likelihood and intensity of TR events [12,13]. However, given the large number of cells within a battery system, the probability of TR is always present, and even a single cell failure can trigger a pack-level TR, potentially leading to catastrophic fires or casualties [14]. Consequently, system-level safety control is essential, focusing on strategies to prevent thermal failure from propagating beyond the initial failure point. A key challenge in this approach lies in determining whether pre-designed safety measures can effectively address real-world accident scenarios. Therefore, validating battery system safety through TP testing becomes indispensable [15–17].

The TP test is aimed at evaluating and verifying the safety of battery systems (see Table 1). It recommends triggering a single cell into TR to assess the risk of TP in the LIB systems, and the system designer is obliged to demonstrate that appropriate countermeasures have been taken to mitigate the related consequent hazards. The rationale of the TP test has been universally acknowledged, and regulatory forums such as Electric Vehicle Safety-Global Technical Regulation (EVS-GTR) [14] and International Standard Organization-Road Vehicles (ISO/TC 22) have been working for years to improve and revise the TP test to promote battery system safety. The TP test involves intentionally triggering one cell into failure and requires the battery system to possess a certain capacity to withstand thermal failure [18].

Current TP test methods require specific trigger mechanisms to initiate TR in target cells [19]. An ideal trigger method should exhibit high repeatability, minimal additional energy input, broad applicability, and minimal system modification. State-of-the-art triggering methods specified in regulatory standards such as ISO 6469-1: 2020/AMD1 [5], SAE J2464: 2021 [7], IEC 62619: 2022 [14], UL 9540A: 2019 [15], and GB 38031: 2020 [16] primarily include heating, nail penetration, and overcharge (see Table 1).

In this study, we developed a high-frequency (HF) induction heating method that uses a smaller, customized inductor coil ($\Phi 18$ mm) to rapidly heat the electrode and induce TR. This method leverages the skin effect of high-frequency electromagnetic induction to achieve rapid heating of highly thermally and electrically conductive metals. However, its implementation in battery systems presents structural challenges that must be carefully addressed. Addressing these challenges, this study investigated TP tests on Ni9-series high-specific-energy battery systems using high-frequency induction heating triggers. The experimental work focuses on three aspects:

- TR triggering at different cell positions: investigating the impact of trigger position on TP through electromagnetic induction heating at various locations;
- Module modification and trigger position selection: optimizing trigger points based on battery system structure and target cell locations;
- System-level TP measurements: conducting TP tests at both module and pack levels to analyze propagation patterns and speeds.

Through these experiments, this study validated the feasibility of electromagnetic induction heating as a TP testing method and provides valuable insights for developing standardized TP test procedures.

Table 1. An overview of current standards incorporating thermal propagation evaluation tests [20].

Standard	Scope	Requirement for Thermal Propagation Test	Trigger Method	Test Procedure	Safety Criteria
IEC 62619: 2022 [21]	Electrical energy storage system, emergency power, uninterrupted power supplies, railway vehicles, marine vehicles, and road vehicles.	Evaluates the response of a battery system against a single cell thermal runaway event, and it does not result in a battery system fire or explosion.	Laser: (first choice) all kinds of laser devices are allowed. (Within 10 min). Heating: -Heating by heater; -Heating by burner; -Heating by inductive heating. -Overcharge, nail penetration, or combination of the above.	Taking laser heating triggering as an example: Cell test (preliminary test): -Fully charge the cell and use a laser beam to torch the cell until rapid temperature increase is observed due to thermal runaway; -Repeat the process three times. If thermal runaway is confirmed on each test with the same conditions, proceed to the battery system test with the same irradiation condition. Battery system test (main test): -Fully charge the battery system and select the target cell; -Use a laser beam to heat the target point until rapid temperature increase due to thermal runaway is observed, and then, turn off the laser; -Observe the battery system for a minimum of 1 h.	No external fire from the battery system, and no battery system case rupture.
UL 9540A: 2019 [22]	Battery energy storage systems (cell level, module level, unit level, and installation level).	Evaluates the fire and explosion hazard characteristics of battery energy storage systems that have the capability to undergo thermal runaway.	-Heating (film heater with surface rate of 4–7 °C/min) If it does not cause thermal runaway, then pick one of the following: -Mechanical (e.g., nail penetration). -Electrical (overcharging, over-discharging, or external short-circuiting). -Alternating heating sources (e.g., oven).	Taking the module test as an example: Module test: -Module shall be charged to 100% SOC; -Select a cell and force it into thermal runaway with maximum heat exposure; -During triggering process, ensure the occurrence of thermal runaway; -The chemical heat release rate, the vent gas composition, the hydrocarbon content, and the smoke release rate shall be calculated or measured.	Thermal runaway is judged at module level, and the vent gas should be nonflammable.
GB 38031: 2020 [23]	Electric vehicle power battery system.	Assess whether the electric vehicle battery system can provide passengers with at least 5 min of escape time upon the event of thermal runaway.	-Heating (heating the back side up to 300 °C or until thermal runaway). -Nail penetration (steel, Φ3–8 mm, angle 20°~60°, 0.1 mm/s~10 mm/s).	-Battery system shall be fully charged to 90%~95% state-of-charge; -Trigger the cell at the geometry center or surrounded by other cells; -Recommended criterion for the thermal runaway judgment: (a) voltage drop to 25%; (b) temperature of monitoring point above the maximum onset thermal runaway temperature given by manufacturer; (c) a temperature rise rate of monitoring point above 1 °C/s, lasting for more than 3 s.	5 min early warning is essential before the occupant is harmed or no propagation.

Table 1. Cont.

Standard	Scope	Requirement for Thermal Propagation Test	Trigger Method	Test Procedure	Safety Criteria
SAE J 2464: 2021 [24]	Various rechargeable energy storage systems (module or pack level).	Evaluate the response of battery system to a single cell thermal runaway event to determine if thermal runaway will propagate to adjacent cells.	- Heating (to 400 °C or until cell thermal runaway, using resistive heating or thermal conductive heat transfer).	<p>Single cell failure propagation test (module or pack level):</p> <ul style="list-style-type: none"> -Fully charged to 100% SOC, stabilized at the maximum operating temperature; -Heat the target cell to 400 °C as fast as possible; -Target cell location selection: (a) the geometric corner of the module or pack; (b) the midpoint of an edge; (c) the center of one face; -Other methods to trigger thermal runaway in one cell are allowed, and the methods to trigger thermal runaway should have minimal influence on the neighboring cells; 	None.
ISO 6469-1: 2020/AMD1 [25]	Lithium-ion-based rechargeable energy storage system.	Demonstrate the behavior of a rechargeable energy storage system or its sub-systems in case of internal short circuit or thermal runaway caused by internal failure of a single cell, and evaluate the after-failure performance.	<ul style="list-style-type: none"> -Internal heater (for cell manufacturers only). -Localized external heating (varies with different chemistries or cell structure). -Nail penetration (cannot be applied to any position in battery system. Only the cells at outmost can be selected). 	<ul style="list-style-type: none"> -The selection of a single cell depends on the chosen trigger method; -Installation of a trigger for the target cell shall not impede the functionality of the original cell or rechargeable energy storage system (RESS) design and its safety features, such as venting, cooling, battery management system, gas permeability, spacing between cells, or other components and thermal barriers; -Criteria of a thermal runaway event: <ul style="list-style-type: none"> (a) temperature exceeding the normal operating range; (b) temperature rise $dT/dt > 15 \text{ K/s}$; (c) supplementary criteria (voltage drop, fire, venting gas or smoke, or occurrence of ejected solid material). 	<p>Critical review is required.</p> <ul style="list-style-type: none"> -Evaluation of the implementation process required for the risk mitigation activities. -Evaluation of the effectiveness of the risk mitigation measures.

2. Methods and Experiments

2.1. The Mechanism of the Induction Heating

The basic principles of electromagnetic induction were first described by Michael Faraday in the 1830s, with subsequent contributions from physicists including Emil Lenz and Joseph Henry. James Clerk Maxwell later unified these electromagnetic phenomena in his famous equations [26]. Induction heating, as a precise, repeatable, and safe non-contact heating method for electrically conductive materials, involves complex interactions between electromagnetic energy and heat transfer [27]. The fundamental mechanism of induction heating is illustrated in Figure 1A. When alternating current (AC) passes through an induction coil, it generates alternating magnetic fields (AMFs). According to Faraday's law of induction, these AMFs induce eddy currents (ECs) in adjacent conductors. The induced ECs generate a secondary magnetic field that opposes the applied AMFs. As these ECs flow through an electrically conducting material, they convert electrical energy into heat. In LIBs, this process occurs when ECs pass through the electrically conductive components (positive and negative electrodes), resulting in Joule heating, as shown in Figure 1B.

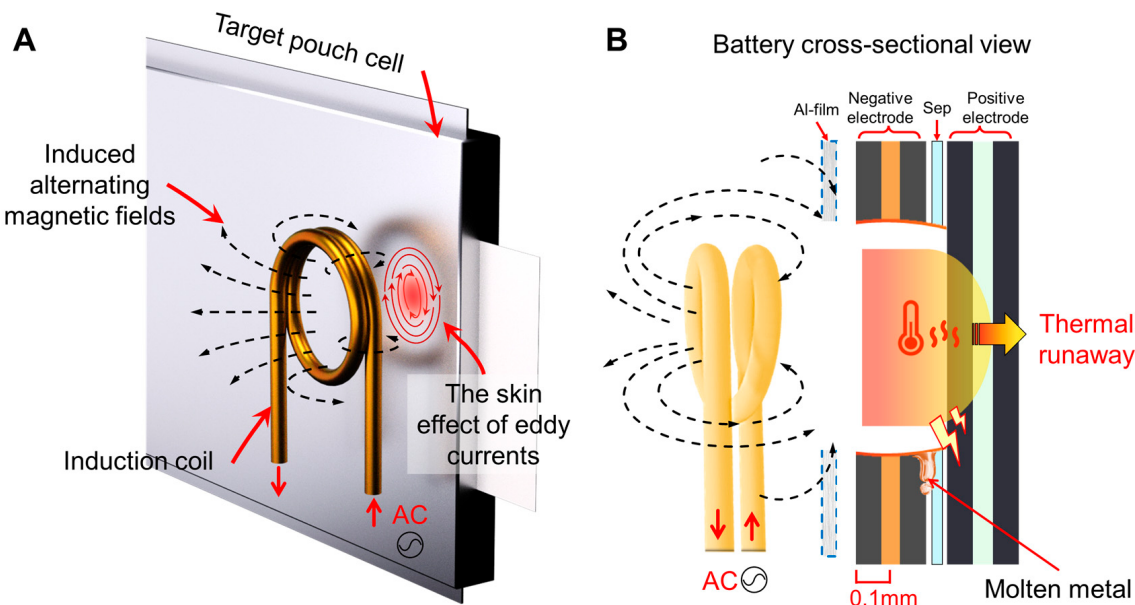


Figure 1. (A) Fundamental mechanism of induction heating for thermal runaway triggering in lithium-ion batteries. (B) Skin effect manifestation during high-frequency induction heating for pouch cell thermal runaway initiation.

A key phenomenon in this process is the skin effect, which becomes prominent at high frequencies (HF). The skin effect causes ECs to concentrate near the conductor's surface, significantly increasing their density (Figure 1A). This concentration enables rapid heating of very thin sections (~ 0.1 mm) with high power density. Although aluminum and copper, commonly used in LIBs, are typically difficult to heat rapidly due to their high thermal conductivity, the skin effect facilitates quick melting of the LIB package. This can lead to heating or melting of the anode or cathode, ultimately causing internal short circuit (ISC) and thermal runaway (TR) simultaneously.

2.2. The Preliminary Induction Heating Tests at Cell Level

The effectiveness of the triggering method in inducing TR in target cells is crucial for conducting a system-level TR propagation test. This study began with a series of preliminary TR triggering experiments on individual cells using high-frequency electromagnetic induction heating. The test subject was a 75 Ah pouch cell, with experiments conducted at two distinct target positions (Target Position 1: center of large surface; Target Position 2: side edge), as shown in Figure 2. A $\Phi 1$ mm armored thermocouple was installed approximately 20 mm from the centroid of each triggering position to monitor temperature changes (Figure 2A).

The initial tests were performed on a 0% state-of-charge (SOC) sample cell at Position 1. To maintain consistency with the module configuration, a 1 mm thick mica sheet was placed between the inductor and the battery (Figure 2B). Post-test examination of the 0% SOC sample cell (Figure 2C) revealed that a 2 s induction heating period successfully compromised both the aluminum laminate casing and multiple electrode layers of the pouch cell, aligning with the theoretical mechanism illustrated in Figure 1B. Further experiments were conducted on 100% SOC sample cells, with the experimental setup shown in Figure 2D,E.

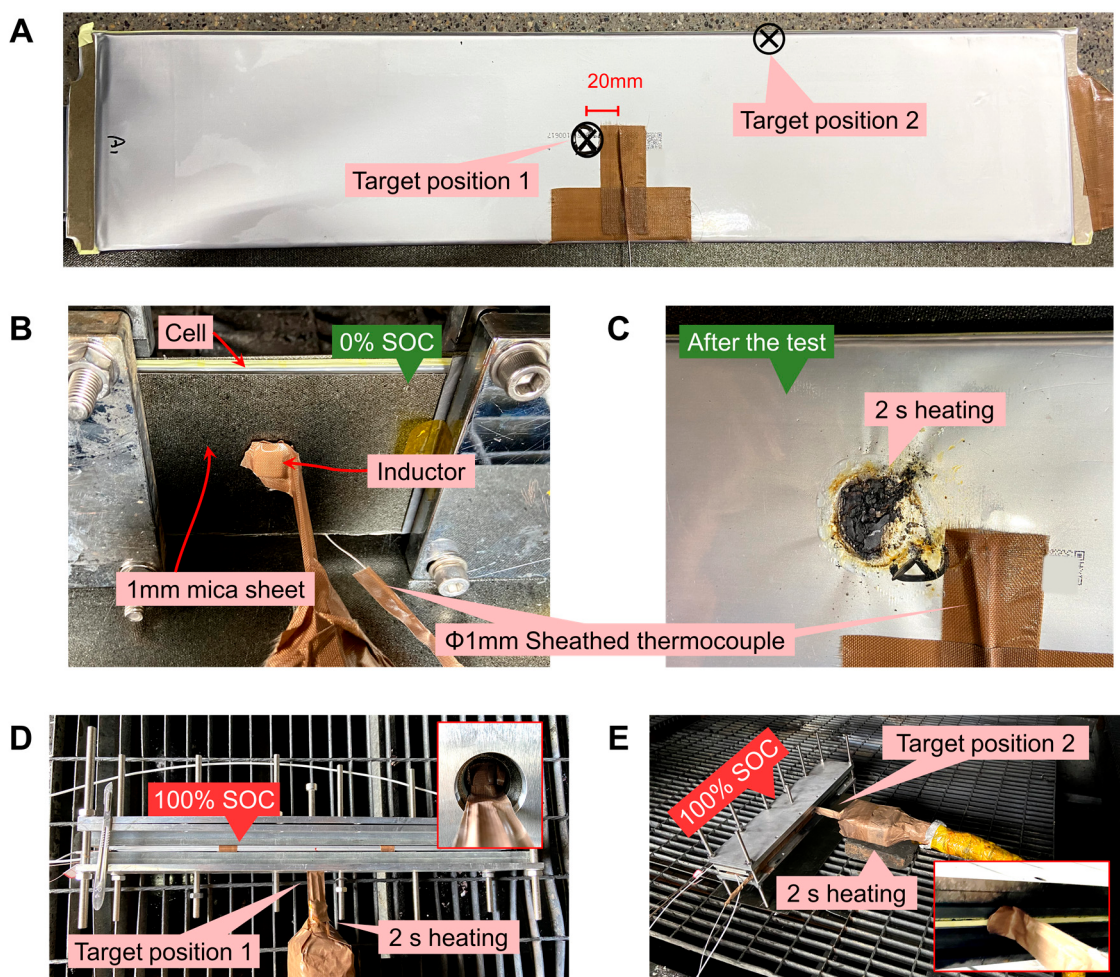


Figure 2. Induction heating-based thermal runaway triggering tests at cell level. (A) Schematic of 75 Ah pouch cell showing two trigger positions: Position 1 (center) and Position 2 (edge). (B) Experimental setup for 0% state-of-charge (SOC) cell with mica sheet insulation during induction heating. (C) Post-test condition after 2 s induction heating, showing penetration through aluminum laminate casing. (D) Thermal runaway triggering at center position (Position 1) for 100% SOC cell. (E) TR triggering at edge position (Position 2) for 100% SOC cell.

2.3. Test Setup for Induction Heating Test at System Level, Box 01

To facilitate system-level TP tests, modifications were made to the target trigger module while maintaining its core functionality. The modification process of Target Trigger Module 01, as shown in Figure 3A, involved creating a 45 mm diameter access opening on the module sidewall by removing protective plates. Armored thermocouples were then installed near the target trigger position and secured with a mica ring (23 mm inner diameter). The installation was finalized using heat-resistant pads within the module, ensuring proper dimensional matching between the induction coil and the installation aperture.

The internal configuration of Box 01 was designed to optimize both experimental validity and cost efficiency, as illustrated in Figure 3B. Only the trigger module contained actual cells at 100% state of charge (SOC), while adjacent modules were aluminum dummies. Gas sensors were strategically positioned throughout the box, and critical safety features were implemented, including explosion-proof (EP) valves and coil access ports on the box sidewall.

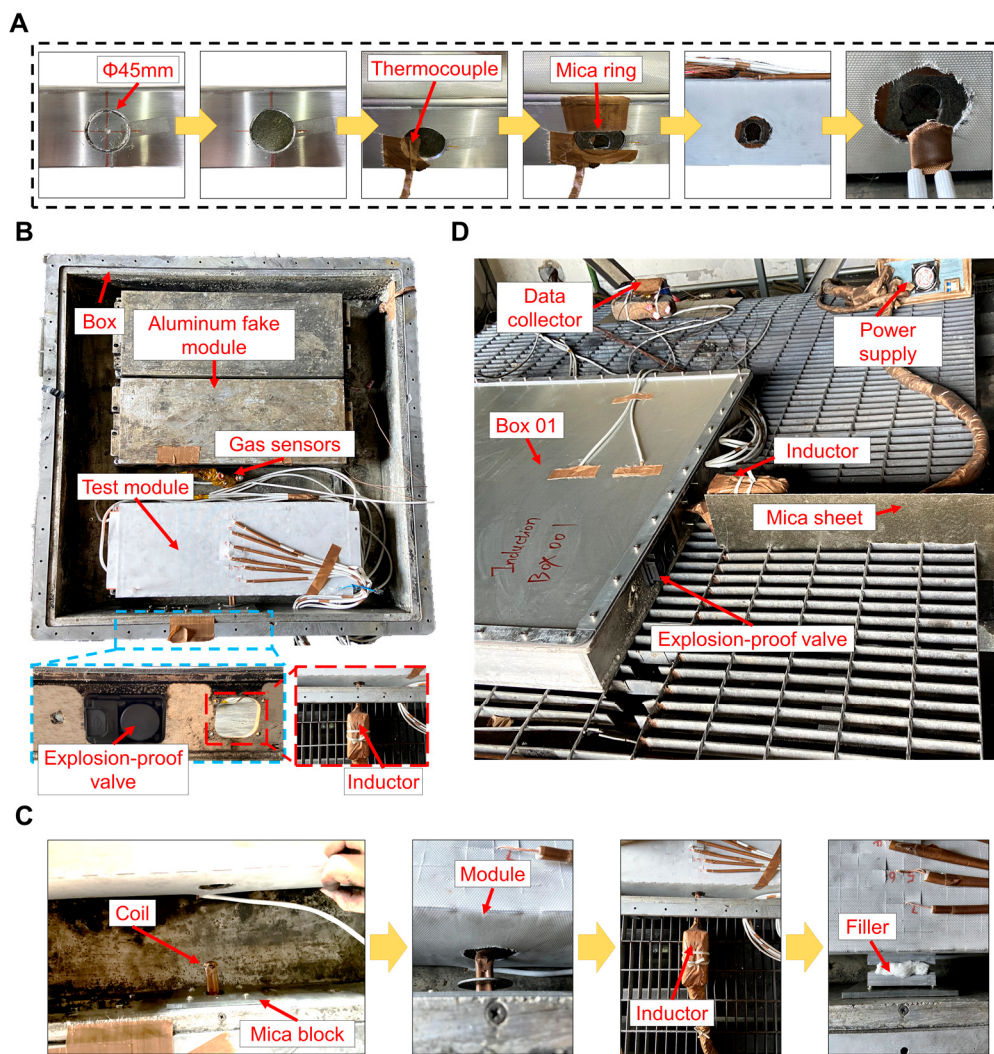


Figure 3. System-level thermal propagation test setup for Box 01. (A) Sequential process of module modification and inductor installation. (B) Test module arrangement showing one active module and two fake modules. (C) Pass-hole resealing process incorporating multi-layer insulation. (D) Completed test platform setup prior to Box 01 test.

To maintain system integrity during testing, a sophisticated coil penetration sealing system was developed (Figure 3C). This system employed a multi-layer barrier approach using mica-based insulation sheets and ceramic thermal padding, which provided both electrical isolation and gas-tight sealing at penetration points. This design was crucial for maintaining box pressure containment during TR events. All thermocouples were routed through the box sidewall and connected to the data collector. The test platform was equipped with a power supply for the induction heating coil. As shown in Figure 3D, the completed test platform setup included a sealed box, power supply, and data acquisition system. The inductor was installed through the box sidewall adjacent to the EP valve, with custom mica blocks and thermal insulation materials used for hole sealing. Additional mica sheet protection was implemented to guard against potential valve exhaust flames.

2.4. Test Setup for Induction Heating Test at System Level, Box 02

To validate the reproducibility of the TP test results, a replicate experiment was conducted using Box 02. This setup maintained an identical configuration to Box 01, with the sole difference being the omission of gas sensors. The modification and setup process followed the same rigorous protocol as previously established.

The modification of Target Trigger Module 02, as illustrated in Figure 4A, began with creating a 45 mm diameter opening on the module sidewall for inductor access. Armored thermocouples were then installed near the target trigger position, followed by securing the installation with a mica ring (23 mm inner diameter) and heat-resistant pads. The internal arrangement of Box 02 (Figure 4B) mirrored that of Box 01, with the trigger module containing actual cells at 100% state of charge (SOC) positioned centrally, flanked by two aluminum fake modules to maintain structural integrity while optimizing cost efficiency.



Figure 4. Test setup of the thermal propagation test at system level, Box 02. (A) The module modification process and the installation of inductor. (B) The same arrangement of the test module and fake modules. (C) The resealing process of the pass hole on the box. (D) The resealed Box 02 with a new box cover.

The coil penetration point was sealed using the established multi-layer protocol (Figure 4C), incorporating mica-based insulation sheets and ceramic thermal padding. This comprehensive sealing system ensured both electrical isolation and pressure containment during TR events. The assembly was completed with a new box cover (Figure 4D), featuring essential safety components including EP valves and secured access ports. This replication study was designed to verify the consistency and reliability of the induction heating trigger method in TP test while maintaining testing conditions identical to those used in Box 01.

3. Result and Discussion

3.1. Results of the Pretest of 100% SOC Cell

The preliminary tests conducted on individual cells at 100% state of charge (SOC) demonstrated the effectiveness and consistency of the induction heating trigger method. Figure 5 presents the comprehensive test results, including temperature–voltage profiles and corresponding visual/thermal imaging documentation.

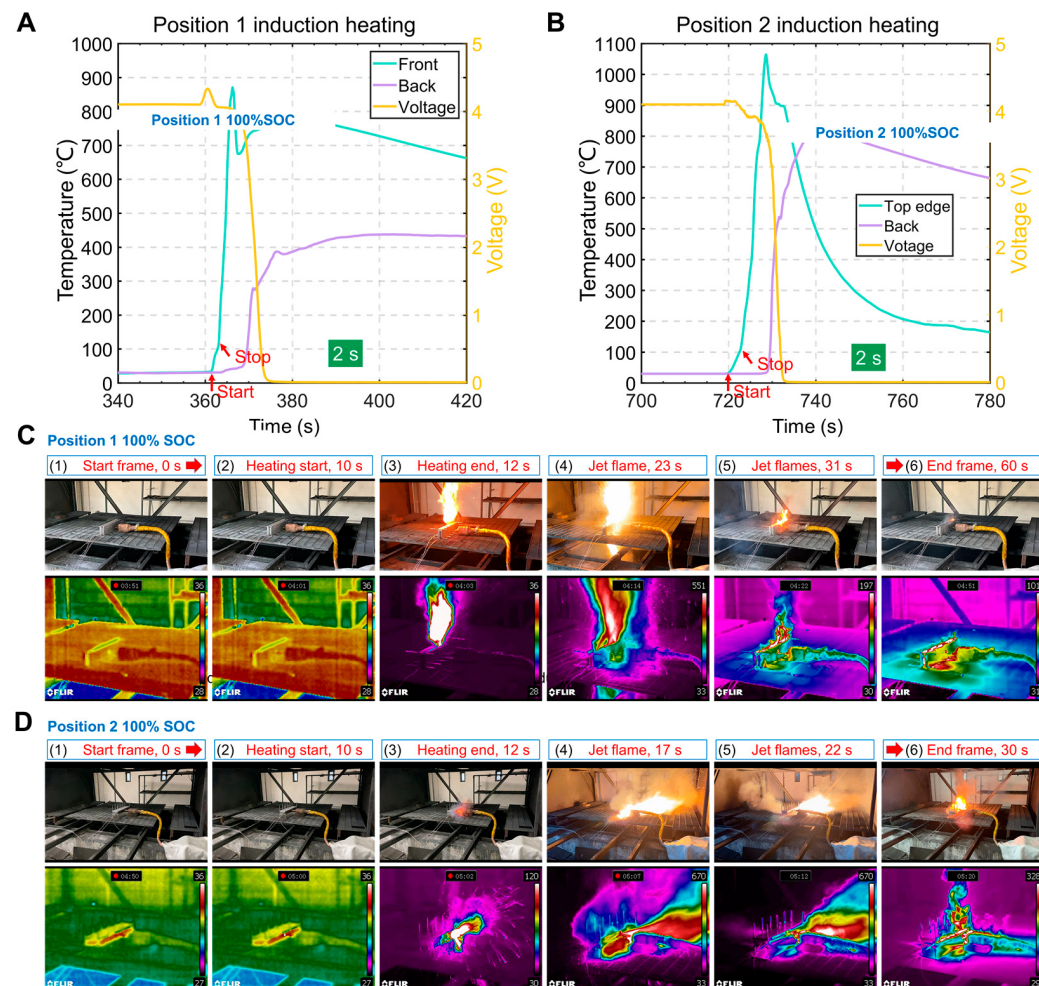


Figure 5. Preliminary test results of thermal runaway triggering on 100% SOC cells. (A) Temperature and voltage profiles during thermal runaway (TR) triggering at Position 1 (center position). (B) Temperature and voltage profiles during TR triggering at Position 2 (edge position). (C) Sequential video capture showing TR event progression from initiation to completion. (D) Corresponding infrared thermal imaging sequence documenting temperature evolution during TR event.

Temperature and voltage measurements from Position 1 (center position) are shown in Figure 5A. The “Front” temperature curve represents measurements from the armored thermocouple near the trigger point, while the “Back” curve indicates the temperature at the cell’s geometric center on the opposite side. For Position 2 (edge position), Figure 5B displays similar measurements, with “Top edge” indicating temperature near the trigger point at the cell edge and “Back” representing the center temperature on the opposite side.

A 2 s induction heating duration consistently triggered TR in both test positions, demonstrating the method’s reliability and reproducibility. This consistent triggering capability is particularly significant for a standardized TP test, as it validates the electromagnetic induction heating method’s effectiveness under identical triggering conditions.

The TR event progression is documented through video and infrared imaging sequences (Figure 5C,D). The thermal event evolved through several distinct stages: initial state (0 s), induction heating initiation (10 s), heating completion (12 s), intense TR phase showing violent thermal events, and final state (60 s). These results validate the electromagnetic induction heating method as a reliable and efficient approach for triggering TR in high-energy lithium-ion cells, establishing a solid foundation for subsequent system-level TP tests.

3.2. Results of the Thermal Propagation Test, Box 01

The TP test of Box 01 was conducted following the previously described experimental setup. The trigger module's cross-sectional structure (Figure 6A) consisted of 24 fully charged cells numbered sequentially, with cell 1 designated as the trigger cell. The module configuration included 1 mm thick mica boards and aluminum side plates at both ends (cells 1 and 24). Thermal barriers were placed between each pair of cells, with an additional aerogel pad between cells 10 and 11. Seven thermocouples (GG-K-30), labeled T1–T7, were embedded within the module, while T0 was an armored thermocouple installed near the trigger position.

The temperature–voltage profiles (Figure 6B) revealed the TR progression through distinct phases. Following 2 s induction heating, T0 rapidly reached 1211 °C, confirming successful TR initiation in cell 1, before dropping due to likely thermocouple detachment. After approximately 11 s, the voltage reading dropped to 0 V due to the severance of the module's positive voltage wire by intense jet flames, preventing further voltage measurements.

The TP sequence revealed distinct phases of progression through the module. T1 began rising at 916.3 s and reached TR at 948.5 s, indicating a propagation time of approximately 44 s between the first two cells. The propagation continued with T2 starting to increase at 1040 s and reaching its peak when T5 began rising at 1082 s. This shows that cells 3–6 underwent complete TP in about 132 s, averaging 33 s per cell. Around the 1100 s mark, the temperature readings became chaotic, with T6, T5, T7, T3, and T4 showing disordered temperature rises due to intense jet flames. The propagation concluded at approximately 1250 s, with a total duration of 350 s (averaging 14.6 s per cell), demonstrating significant acceleration in propagation rate. Gas sensor data (Figure 6B inset) provided additional insights into the TR process. Volatile organic compounds (VOCs), CO, and CO₂ sensors detected gas evolution within 2 s of trigger initiation, with CO showing the fastest response. While VOC and CO readings quickly reached detection limits before sensor failure at 950 s, CO₂ measurements continued even after other sensors failed.

The progression of the TR event is clearly shown in Figure 6C. Beginning at 900 s with the initiation of induction heating, the sequence captured key events, including visible flames at the inductor penetration point at 902 s, the onset of cell TR at 904 s, and the activation of the EP valve at 908 s, which resulted in intense jet flames extending approximately 2 m. These intense jet flames persisted throughout the remainder of the TR propagation process until the final cell's failure.

3.3. Results of the Thermal Propagation Test, Box 02

The Box 02 test was conducted as a parallel verification test with an identical trigger module structure to Box 01, as illustrated in Figure 7A. The temperature and voltage profiles recorded during the test are presented in Figure 7B. The induction heating was initiated at 720 s and terminated after 2 s, successfully triggering TR in the target cell, as evidenced by the T0 temperature curve.

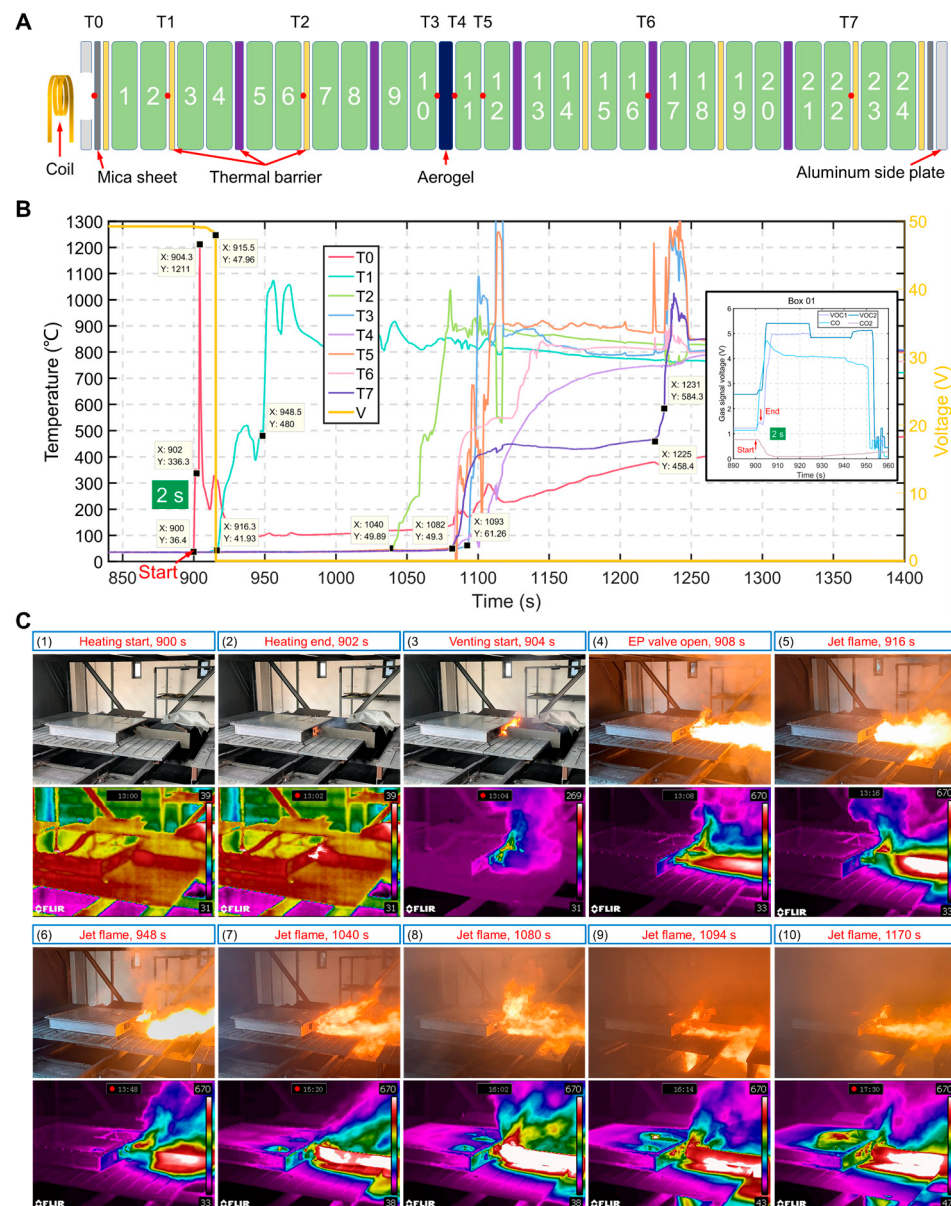


Figure 6. System-level thermal propagation test results for Box 01. (A) The relative positions of the cells, thermocouples, and thermal barriers inside the battery module. (B) The temperature and voltage results of the Box 01 test with the four gas sensors. (C) The snapshots of normal and infrared videos, showing the thermal runaway propagation process from initiation to completion with continuous jet flames.

The TP displayed distinct phases with varying progression rates. Initial propagation began with T1's rapid temperature rise at 733.3 s, followed by cell 3's TR around 770 s. The sequence continued to T2 (rising at 885.2 s), marking cell 6's TR. The first six cells completed their TR sequence in approximately 165 s, averaging 27.5 s per cell. By the time T3 surged at 983.8 s (indicating cell 10's TR), the average propagation time for the first ten cells was 26.4 s per cell.

A significant interruption in the TP occurred after cell 10, during which T1–T3 temperatures gradually decreased, while T4 slowly rose from room temperature to 240.6 °C. This pause lasted until 1424 s, when T4 showed a sudden temperature surge, indicating TR in cell 11. The final phase of propagation began at 1609 s with T7's temperature rise, culminating around 1620 s when the voltage dropped to 0 V. Notably, the propagation through cells 11–24 occurred more rapidly, taking approximately 194 s with an average

of 14 s per cell, significantly faster than the initial propagation rate. This acceleration in propagation speed, despite the approximately 440 s delay caused by the aerogel pad between T3 and T4, can be attributed to the preheating of the remaining cells during the extended pause. The voltage data, which were successfully recorded throughout this test, showed approximately 12 distinct drops, corresponding to the parallel-connected cell pairs. The final three voltage drops occurred in rapid succession, indicating particularly intense and swift TR propagation in the final stages.

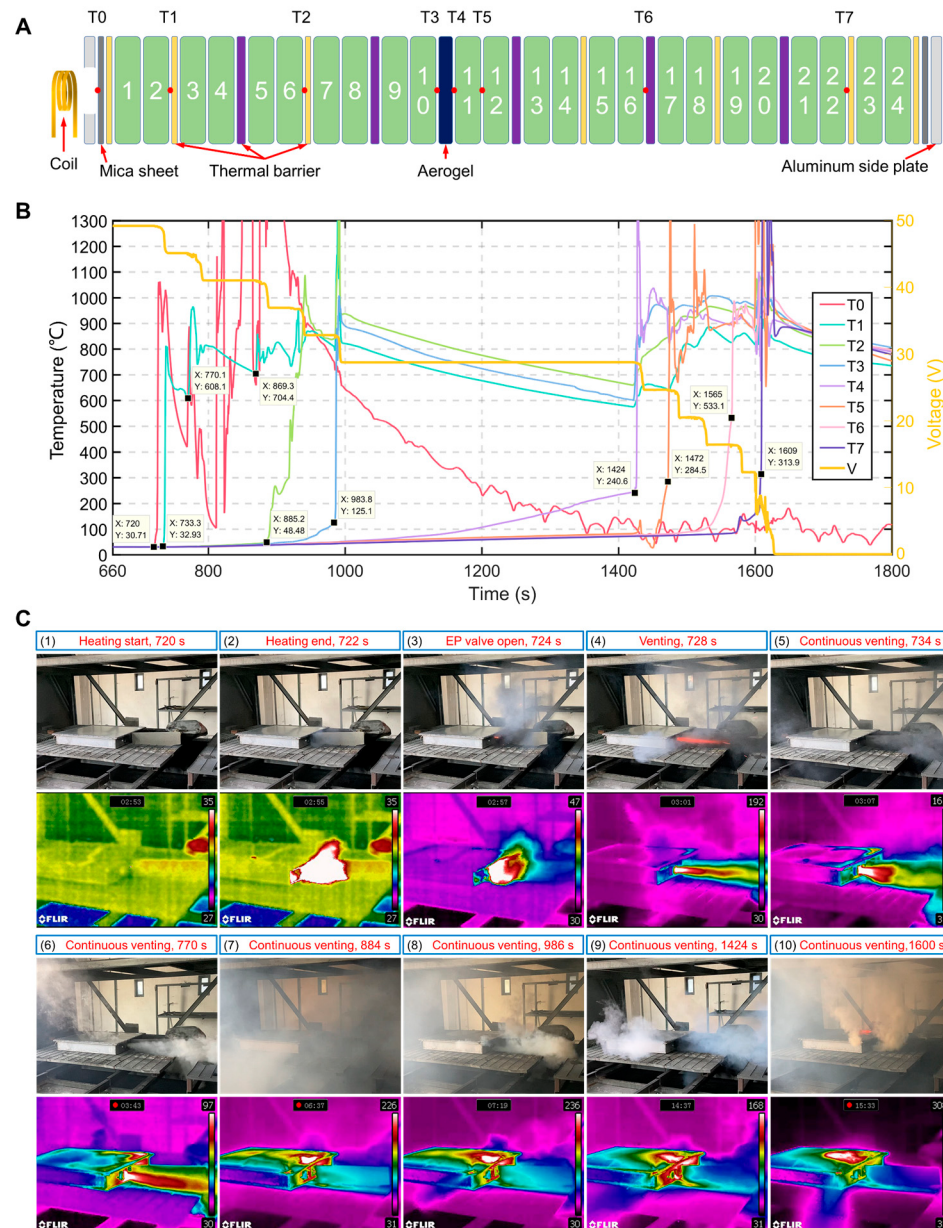


Figure 7. System-level thermal propagation test results for Box 02. (A) The relative positions of the cell, thermocouples and thermal barriers inside the battery module. (B) The temperature result of the Box 02 test. (C) The snapshots of normal and infrared videos for Box 02.

Figure 7C presents a series of 10 video/infrared video snapshots captured at different time points during the Box 02 test. Frame (1) shows the initiation of induction heating at 720 s. Frame (2), taken at 722 s, marks the end of induction heating, where the EP valve remained closed. Two seconds later, as shown in frame (3), the EP valve opened. In frame (4), at 728 s, intense venting from the battery was observed, producing a jet of sparks at the EP valve location, though the box remained free from overall fire. Frames (5) through

(10) document the subsequent progression of the test through video/infrared imagery, showing that even after all batteries underwent TR, Box 02 maintained its integrity without catching fire.

4. Discussion

The experimental results demonstrate that high-frequency induction heating serves as an effective and reliable method for system-level TP tests of LIBs. This approach exhibits several distinct advantages in triggering TR. The consistent 2 s heating duration successfully initiated TR in both Box 01 and Box 02 tests, ensuring that subsequent TP dynamics were determined by the battery system's inherent characteristics rather than the triggering method. The method provides precise energy control, minimal mechanical intrusion, and real-time monitoring capabilities while maintaining a clean thermal interface without introducing foreign materials.

The box-level testing methodology incorporating dummy modules proved to be an efficient approach for validating TP characteristics within modules. This cost-effective strategy allows for detailed examination of thermal barrier performance and propagation patterns at the module level. However, comprehensive evaluation of system-level TP behavior ultimately requires testing with complete battery systems, as system-level interactions and thermal management features can significantly influence propagation dynamics.

The divergent results between Box 01 and Box 02 tests primarily stem from differences in box sealing quality. Inadequate sealing in Box 01 led to flame formation, which enhanced heat transfer through convection and radiation, resulting in accelerated TP. In contrast, Box 02's proper sealing prevented oxygen ingress and flame formation, enabling observation of the thermal barriers' effectiveness in delaying sequential propagation. The aerogel thermal barrier demonstrated significant capability in retarding propagation, as evidenced by the 440 s delay between cells 10 and 11 in Box 02, highlighting the importance of proper thermal isolation materials.

Based on these findings, several key recommendations emerge for TP management in battery systems. First, the development of cost-effective thermal barriers with enhanced insulation properties is crucial for managing solid-state heat conduction between modules. Second, advanced gas flow management systems, either within the box or through strategic vent valve placement, are essential for isolating high-temperature combustible gases from battery modules, thereby reducing temperature rise and fire risks. Finally, efficient heat dissipation systems should be implemented to rapidly transfer heat from the box interior to the external environment. This comprehensive approach to thermal management, combining thermal barriers, gas management, and active cooling, provides a robust strategy for enhancing battery system safety.

5. Conclusions

This study presents a comprehensive investigation of TR propagation in large-format battery systems, with significant findings in testing methodology development and thermal propagation characterization. The main contributions can be summarized in three aspects: First, we developed and validated an high-frequency electromagnetic induction heating method for system-level thermal propagation test. The method demonstrated excellent reliability and precision with consistent 2s triggering duration, providing controlled initial conditions for TR studies. This advancement establishes a foundation for standardized testing protocols in battery system safety test and evaluation.

Second, through parallel box-level TP tests using both real and fake modules, we established an efficient approach for validating thermal protection strategies. This testing methodology revealed that system sealing quality fundamentally determines propaga-

tion mechanisms. In inadequately sealed systems, the formation of open flames leads to accelerated propagation through enhanced convective and radiative heat transfer. Conversely, proper sealing maintains an oxygen-deficient environment, resulting in controlled sequential propagation patterns.

Finally, our findings provide practical insights for thermal management system design in large-format batteries. The results emphasize the importance of a comprehensive protection strategy incorporating the following: (1) effective thermal barriers for managing solid-state heat transfer, (2) advanced gas management systems for isolating high-temperature combustible gases, and (3) efficient heat dissipation systems for rapid thermal energy removal. These design considerations are crucial for enhancing battery system safety in practical applications.

These contributions advance both the understanding of TR propagation mechanisms and the development of safety validation methods. The findings and methodology presented here support the establishment of more rigorous safety standards and testing protocols, promoting safer implementation of large-format battery systems.

Author Contributions: C.J.: Conceptualization, Data Curation, Methodology, Investigation, Writing—Original Draft. J.G.: Resources, Visualization. C.X.: Formal Analysis, Validation. W.W.: Resources, Investigation. L.L.: Conceptualization, Supervision, Project Administration. X.F.: Supervision, Methodology, Formal Analysis, Funding Acquisition, Writing—Review & Editing. All authors have read and agreed to the published version of the manuscript.

Funding: This work is supported by the National Key Technologies Research and Development Program Scientific and Technological Strategic Innovation Cooperation (#2022YFE0207900). This work is supported by the Innovative Research Group Project of the National Natural Science Foundation of China [52076121, 52106284].

Data Availability Statement: Data are available from the corresponding author: fxn17@mail.tsinghua.edu.cn (X.F.).

Conflicts of Interest: Authors Jiangna Gu, Wanlin Wang and Lirong Liu were employed by the Farasis Energy (GanZhou) Co., Ltd. The remaining authors declare that the research was conducted in the absence of any commercial or financial relationships that could be construed as a potential conflict of interest.

References

1. Li, M.; Lu, J.; Chen, Z.; Amine, K. 30 years of lithium-ion batteries. *Adv. Mater.* **2018**, *30*, 1800561. [[CrossRef](#)] [[PubMed](#)]
2. Ouyang, D.; Chung, Y.H.; Liu, J.; Bai, J.; Zhou, Y.; Chen, S.; Shu, C.M. Characteristics and mechanisms of as well as evaluation methods and countermeasures for thermal runaway propagation in lithium-ion batteries. *Prog. Energy Combust. Sci.* **2025**, *108*, 101209. [[CrossRef](#)]
3. Finegan, D.P.; Billman, J.; Darst, J.; Hughes, P.; Trillo, J.; Sharp, M.; Darcy, E. The battery failure databank: Insights from an open-access database of thermal runaway behaviors of Li-ion cells and a resource for benchmarking risks. *J. Power Sources* **2024**, *597*, 234106. [[CrossRef](#)]
4. Schöberl, J.; Ank, M.; Schreiber, M.; Wassiliadis, N.; Lienkamp, M. Thermal runaway propagation in automotive lithium-ion batteries with NMC-811 and LFP cathodes: Safety requirements and impact on system integration. *eTransportation* **2024**, *19*, 100305. [[CrossRef](#)]
5. Jin, Y.; Meng, D.; Zhao, C.-X.; Yu, J.-L.; Wang, X.-H.; Wang, J. Experimental Study on Thermal Runaway Characteristics of High-Nickel Ternary Lithium-Ion Batteries under Normal and Low Pressures. *Batteries* **2024**, *10*, 287. [[CrossRef](#)]
6. Shi, C.; Wang, H.; Shen, H.; Wang, J.; Li, C.; Li, Y.; Xu, W.; Li, M. Thermal Runaway Characteristics and Gas Analysis of LiNi_{0.9}Co_{0.05}Mn_{0.05}O₂ Batteries. *Batteries* **2024**, *10*, 84. [[CrossRef](#)]
7. Wang, Z.; Li, L.; Heo, H.; Ren, L.; Wei, Y.; Lee, K.; Tian, H.; Xu, Z.; Sun, Z.; Kim, T.; et al. Synthesis and characterization of core–shell high-nickel cobalt-free layered LiNi_{0.95}Mg_{0.02}Al_{0.03}O₂@Li₂ZrO₃ cathode for high-performance lithium ion batteries. *J. Colloid Interface Sci.* **2024**, *666*, 424–433. [[CrossRef](#)]
8. Wang, S.; Zhang, C.; Chen, D.; Qin, Y.; Xu, L.; Li, Y.; Wang, Q.; Feng, X.; Wang, H. Explosion characteristics of two-phase ejecta from large-capacity lithium iron phosphate batteries. *eTransportation* **2024**, *22*, 100377. [[CrossRef](#)]

9. Wang, Q.; Wang, H.; Xu, C.; Jin, C.; Wang, S.; Xu, L.; Ouyang, J.; Feng, X. Multidimensional fire propagation of lithium-ion phosphate batteries for energy storage. *eTransportation* **2024**, *20*, 100328. [[CrossRef](#)]
10. Wang, R.; Liu, G.; Wang, C.; Ji, Z.; Yu, Q. A comparative study on mechanical-electrical-thermal characteristics and failure mechanism of LFP/NMC/LTO batteries under mechanical abuse. *eTransportation* **2024**, *22*, 100359. [[CrossRef](#)]
11. Tian, J.; Fan, Y.; Pan, T.; Zhang, X.; Yin, J.; Zhang, Q. A critical review on inconsistency mechanism, evaluation methods and improvement measures for lithium-ion battery energy storage systems. *Renew. Sustain. Energy Rev.* **2024**, *189*, 113978. [[CrossRef](#)]
12. Guo, J.-X.; Gao, C.; Liu, H.; Jiang, F.; Liu, Z.; Wang, T.; Ma, Y.; Zhong, Y.; He, J.; Zhu, Z.; et al. Inherent thermal-responsive strategies for safe lithium batteries. *J. Energy Chem.* **2023**, *89*, 519–534. [[CrossRef](#)]
13. Wu, M.; Han, S.; Liu, S.; Zhao, J.; Xie, W. Fire-safe polymer electrolyte strategies for lithium batteries. *Energy Storage Mater.* **2024**, *66*, 103174. [[CrossRef](#)]
14. Shen, R.; Quan, Y.; McIntosh, J.D.; Salem, A.; Wang, Q. Fire Safety of Battery Electric Vehicles: Hazard Identification, Detection, and Mitigation. *SAE Int. J. Electrified Veh.* **2024**, *13*, 279–294. [[CrossRef](#)]
15. Jin, C.; Sun, Y.; Wang, H.; Zheng, Y.; Wang, S.; Rui, X.; Xu, C.; Feng, X.; Wang, H.; Ouyang, M. Heating power and heating energy effect on the thermal runaway propagation characteristics of lithium-ion battery module: Experiments and modeling. *Appl. Energy* **2022**, *312*, 118760. [[CrossRef](#)]
16. Jin, C.; Sun, Y.; Wang, H.; Lai, X.; Wang, S.; Chen, S.; Rui, X.; Zheng, Y.; Feng, X.; Wang, H.; et al. Model and experiments to investigate thermal runaway characterization of lithium-ion batteries induced by external heating method. *J. Power Sources* **2021**, *504*, 230065. [[CrossRef](#)]
17. Mulder, B.; Schöberl, J.; Birke, K.P. Thermal Propagation Test Bench with Multi Pouch Cell Setup for Reproducibility Investigations. *Batteries* **2023**, *9*, 447. [[CrossRef](#)]
18. Mei, J.; Shi, G.; Li, Q.; Liu, H.; Wang, Z. Experimental study on the effect of phase change material on thermal runaway characteristics of lithium-ion battery under different triggering methods. *J. Energy Storage* **2023**, *75*, 109832. [[CrossRef](#)]
19. Kriston, A.; Kersys, A.; Antonelli, A.; Ripplinger, S.; Holmstrom, S.; Trischler, S.; Döring, H.; Pfrang, A. Initiation of thermal runaway in Lithium-ion cells by inductive heating. *J. Power Sour.* **2020**, *454*, 227914. [[CrossRef](#)]
20. Technical Report-Evaluation Tests for Thermal Propagation Resulting from Secondary Battery Thermal Runaway. 2021. Available online: <https://www.test-navi.com/eng/report/pdf/EvaluationTestsForThermalPropagationResultingFromSecondaryBatteryThermalRunaway.pdf> (accessed on 20 February 2025).
21. IEC 62619:2022; Secondary Cells and Batteries Containing Alkaline or Other Non-Acid Electrolytes-Safety Requirements for Secondary Lithium Cells and Batteries, for Use in Industrial Applications. 2022. Available online: <https://webstore.iec.ch/publication/64073> (accessed on 20 February 2025).
22. ANSI/CAN/UL 9540A; Standard for Safety-Test Method for Evaluating Thermal Runaway Fire Propagation in Battery Energy Storage Systems. 2019. Available online: <https://www.shopulstandards.com/ProductDetail.aspx?UniqueKey=36503> (accessed on 20 February 2025).
23. GB 38031-2020; Electric Vehicles Traction Battery Safety Requirements. Available online: http://www.gbstandards.org/GB_standard_english.asp?code=GB%2038031-2020 (accessed on 20 February 2025).
24. SAE J2464-2021; Electric and Hybrid Electric Vehicle Rechargeable Energy Storage System (RESS) Safety and Abuse Testing. 2021. Available online: https://www.sae.org/standards/content/j2464_202108 (accessed on 20 February 2025).
25. ISO 6469-1:2020/Amd 1; Electrically Propelled Road Vehicles-Safety specifications—Part 1: Rechargeable Energy Storage System (RESS)—Amendment 1: Safety Management of Thermal Propagation. Available online: <https://www.iso.org/standard/73574.html> (accessed on 20 February 2025).
26. Bayerl, T.; Duhovic, M.; Mitschang, P.; Bhattacharyya, D. The heating of polymer composites by electromagnetic induction—A review. *Compos. Part A Appl. Sci. Manuf.* **2014**, *57*, 27–40. [[CrossRef](#)]
27. Schaeffler, S.; Jossen, A. In situ measurement and modeling of internal thermal runaway propagation within lithium-ion cells under local overheating conditions. *J. Power Sources* **2024**, *614*, 234968. [[CrossRef](#)]

Disclaimer/Publisher’s Note: The statements, opinions and data contained in all publications are solely those of the individual author(s) and contributor(s) and not of MDPI and/or the editor(s). MDPI and/or the editor(s) disclaim responsibility for any injury to people or property resulting from any ideas, methods, instructions or products referred to in the content.